Commun. Comput. Phys.
doi: 10.4208/cicp.OA-2016-0127

Vol. **22**, No. 1, pp. 285-302
July 2017

Study on Mass Transports in Evolution of Separation Bubbles Using LCSs and Lobe Dynamics

Shengli Cao[1], Wei Wang[1], Jiazhong Zhang[1,*] and Yan Liu[2]

[1] *School of Power and Energy Engineering, Xi'an Jiaotong University, Xi'an, 710049, P.R. China.*
[2] *School of Mechanical Engineering, Northwestern Polytechnical University, Xi'an, 710072, P.R. China.*

Received 7 August 2016; Accepted (in revised version) 28 November 2016

Abstract. The lobe dynamics and mass transport between separation bubble and main flow in flow over airfoil are studied in detail, using Lagrangian coherent structures (LCSs), in order to understand the nature of evolution of the separation bubble. For this problem, the transient flow over NACA0012 airfoil with low Reynolds number is simulated numerically by characteristic based split (CBS) scheme, in combination with dual time stepping. Then, LCSs and lobe dynamics are introduced and developed to investigate the mass transport between separation bubble and main flow, from viewpoint of nonlinear dynamics. The results show that stable manifolds and unstable manifolds could be tangled with each other as time evolution, and the lobes are formed periodically to induce mass transport between main flow and separation bubble, with dynamic behaviors. Moreover, the evolution of the separation bubble depends essentially on the mass transport which is induced by lobes, ensuing energy and momentum transfers. As the results, it can be drawn that the dynamics of flow separation could be studied using LCSs and lobe dynamics, and could be controlled feasibly if an appropriate control is applied to the upstream boundary layer with high momentum.

AMS subject classifications: 35Q35, 35Q30, 76G25, 93D05, 86-08

Key words: Mass transport, separation bubble, Lagrangian coherent structures, lobe dynamics.

1 Introduction

Flow separation is a kind of common phenomenon in flow over airfoil, building or blade etc., and it usually leads the airfoil or blade to stall, resulting in negative effects on the aerodynamic performance of airfoil or blade. However, flow separation is still one of the

*Corresponding author. *Email addresses:* csl1993@stu.xjtu.edu.cn (S. L. Cao), weiwwang@foxmail.com (W. Wang), jzzhang@mail.xjtu.edu.cn (J. Z. Zhang), liuyan@nwpu.edu.cn (Y. Liu)

main problems in aerodynamics, and there is a rich variety of nonlinear phenomena in flow separation, such as the evolution of separation bubble.

Some studies have been carried out on the separation of laminar flow since Horton [1] described initially the structure of classical two-dimensional laminar separation bubble. These studies are mainly focused on the formation of separation bubble and the change of lift with angles of attack [2], the structures and behaviors of laminar separation bubbles [3, 4], the vortex shedding phenomena in the flow over airfoil [5,6], the stability of laminar separation bubbles in the flow over airfoil [7-9] and other properties or phenomena in separation bubbles [10-12].

Indeed, for the flow around a body in turbo-machinery and aerospace engineering, the mass transport between separation bubble and main flow has an important influence on the aerodynamic performance of blade and airfoil near stall, and such kind of transport is a dynamic behavior. The nature for such phenomenon is still open, and hence it is necessary to study the evolution of the mass transport between separation bubble and main flow in depth, from viewpoint of dynamics. However, none of the above studies analyzed the separation bubble from the viewpoint of mass transport and energy exchange in the generation, evolution and breaking of the separation bubble. Most of traditional flow field numerical methods are based on Eulerian perspective. However, for the unsteady flow, Eulerian description can only describe the instantaneous state of flow but couldn't reveal the dynamic properties. In fact, flow over a body is a kind of nonlinear dynamic system. Flow separation, which is a kind of Lagrangian behavior, means that the fluid particles are separated from the boundary wall. Conventional Eulerian description is not sufficient to describe and analyze the unsteady flow anymore. Nevertheless, the transport process between the separation bubbles and the free stream can be captured from viewpoint of Lagrangian dynamics.

Recently, using Lagrangian description of the fluid and nonlinear dynamics to study the dynamic behaviors is indeed becoming more and more popular. Van Dommelen [13] studied the boundary layer equation in Lagrangian frame, and he also put forward the flow separation criterion on the basis of Lagrangian dynamics. From the point of view of dynamics, the phenomenon of periodic vortex shedding from the wake of flow over cylinder is numerically analyzed by Shariff et al. [14]. Duan and Wiggins [15] quantitatively described the mass transport between the separation zone and the free stream around circle cylinder by lobe dynamics. However, traditional manifolds in nonlinear dynamics can only be available in infinite-time flow. For the finite-time flow, the concepts of finite-time manifolds and Lagrangian Coherent Structures (LCSs) are proposed by Haller [16] to define the separatrix of different basins in finite-time flow. Haller [17] and Shadden [18] proposed using LCS as the transport boundary. Following that, Lei [19] numerically simulated the mass transport in transient flow over impulsively started circular cylinder by LCS. Currently, the LCS has been widely used to study the various flow phenomena, such as separation [20, 21] oceanic flow [22], turbulence [23] and atmospheric flow [24], etc.

In this paper, the flows over NACA0012 airfoil are studied numerically, and La-

grangian Coherent Structures and lobe dynamics are introduced to study the mass transport between separation bubble and main flow in the flow over airfoil with low Reynolds number.

2 Lagrangian coherent structures and lobe dynamics

2.1 Lagrangian coherent structures

The flow over an airfoil is a kind of finite-time transient flow. Haller and Yuan [25] proposed finite-time stable and unstable manifolds, which form the Lagrangian coherent structures of the fluid, to act as the boundaries of the different dynamic regions in the flow. For two-dimensional flow, the finite-time stable manifolds are regarded as repelling LCSs because the fact that the stable manifolds have maximum repelling rate and are defined as locally maximum repelling material lines. Similarly, the finite-time unstable manifolds also are regarded as attracting LCSs and are defined as locally maximum attracting material lines. Mathematically, Lyapunov exponent of a dynamical system is a quantity that can characterize the rate of separation of infinitesimally close trajectories. Inspired by this, Haller and Shadden [18] proposed that finite-time Lyapunov exponent (FTLE) can be used to measure the repelling and attracting properties of the finite-time system. On the other hand, the finite-time manifolds can be depicted by the contour plot of FTLE field. Of course, there are other definitions of LCSs and computation strategies proposed by Haller [26] and other researchers [27]. In this paper, the contour plot of FTLE field is used to locate the LCSs in flow field.

The two-dimensional flow can be considered as a dynamical system,

$$\dot{\boldsymbol{x}}(t;t_0,\boldsymbol{x_0})=\boldsymbol{u}(\boldsymbol{x},t),\quad \boldsymbol{x}\in U, \tag{2.1}$$

where $\boldsymbol{u}(\boldsymbol{x},t)$ is the velocity field and $\boldsymbol{x}(t;t_0,\boldsymbol{x_0})$ describe the trajectory of a fluid element starting at initial position $\boldsymbol{x_0}$ at time t_0. The flow domain is denoted by U. The flow of the dynamical system, namely Eq. (2.1), are denoted by,

$$F_{t_0}^t(\boldsymbol{x_0})=\boldsymbol{x}(t;t_0,\boldsymbol{x_0}),\quad \boldsymbol{x}\in U. \tag{2.2}$$

If two fluid particles separated by a small distance at time t_0, and their positions are $\boldsymbol{x_0}$ and $\boldsymbol{x_0}+\delta\boldsymbol{x_0}$, respectively, and then at time t,

$$\delta\boldsymbol{x}=\boldsymbol{x}(t;t_0,\boldsymbol{x_0}+\delta\boldsymbol{x_0})-\boldsymbol{x}(t;t_0,\boldsymbol{x_0})=F_{t_0}^t(\boldsymbol{x_0}+\delta\boldsymbol{x_0})-F_{t_0}^t(\boldsymbol{x_0})=\nabla F_{t_0}^t(\boldsymbol{x_0})\,\delta\boldsymbol{x_0}+o\left(\|\delta\boldsymbol{x}\|^2\right). \tag{2.3}$$

The stretching coefficient between the two particles is denote by,

$$\lim_{|\delta\boldsymbol{x_0}|\to 0}\frac{|\delta\boldsymbol{x}|}{|\delta\boldsymbol{x_0}|}=\sqrt{\boldsymbol{e}^*\cdot\nabla F_{t_0}^t(\boldsymbol{x_0})^*\cdot\nabla F_{t_0}^t(\boldsymbol{x_0})\cdot\boldsymbol{e}}=\sqrt{\boldsymbol{e}^*\cdot C(\boldsymbol{x_0})\cdot\boldsymbol{e}}, \tag{2.4}$$

where $\boldsymbol{e}=\delta\boldsymbol{x_0}/|\delta\boldsymbol{x_0}|$, and superscript * denotes transpose of matrix. $C(\boldsymbol{x_0})$ is the Cauchy-Green strain tensor defined as $C(\boldsymbol{x_0})=\nabla F_{t_0}^t(\boldsymbol{x_0})^*\cdot\nabla F_{t_0}^t(\boldsymbol{x_0})$. For two-dimensional flow, $C(\boldsymbol{x_0})$ is a 2×2 symmetric positive definite matrix, $\boldsymbol{\xi_1}$ and $\boldsymbol{\xi_2}$ denote the eigenvectors of $C(x_0)$, λ_1 and λ_2 are the eigenvalues associated with $\boldsymbol{\xi_1}$ and $\boldsymbol{\xi_2}$, respectively. These eigenvalues and eigenvectors satisfy $0<\lambda_1\leq\lambda_2$, $\boldsymbol{\xi_1}\perp\boldsymbol{\xi_2}$. For incompressible flows, these eigenvalues satisfy $\lambda_1\lambda_2=1$. So, the eigenvalues of $C(\boldsymbol{x_0})$ are not repeated, and the following condition should be satisfied $0<\lambda_1<1<\lambda_2$. The deformation of the fluid clusters includes tension, compression and rotation in different directions, so $C(\boldsymbol{x_0})$ can be used to describe the tension and compression of fluid clusters. In the time interval $|t-t_0|$, FTLE can be expressed by λ_2,

$$\sigma_{t_0}^t(\boldsymbol{x_0})=\frac{1}{|t-t_0|}\ln\sqrt{\lambda_2}. \tag{2.5}$$

The velocity field, which is obtained by numerical computation, is used to integral to get the trajectories of the particles. After obtaining the distribution of FTLE in the flow field, contours that will visualize LCSs in the flow field are plotted. Then, the repelling LCSs can be depicted by the contour plot of FTLE field with $t-t_0>0$, and the attracting LCSs can be depicted by the contour plot with $t-t_0<0$. Detailed definitions and calculations for LCSs can be referred to literature [28].

2.2 Lobe dynamics

A brief introduction to the lobe dynamics is given in the following. For periodic and quasi-periodic dynamical system with period T, a volume- and orientation- preserving *Poincaré* map $PM:M\to M$ is introduced and defined on a two-dimensional phase space M. Consequently, *Poincaré* map can be used to find the fixed points and their invariant manifolds on *Poincaré* section. For the sake of clarity, the hyperbolic fixed points of PM in *Poincaré* section are denoted by p_i with associated stable manifold $W^s(p_i)$ and unstable manifold $W^u(p_i)$, and the unstable manifold between point X and point Y can be denoted by $U[X,Y]$, and the stable manifold by $S[X,Y]$.

A region is a connected subset of M with boundaries, consisting of parts of the boundary of M and segments of stable and unstable manifolds of hyperbolic fixed points. The notion of a "lobe", formed by stable and unstable manifolds of hyperbolic orbits in two-dimensional flows, plays an important role in the study of transport in time-periodic and quasi-periodic flows.

Suppose $q\in W^s(p_2)\cap W^u(p_1)$. If $U[p_1,q]$ and $S[p_2,q]$ intersect only at q, then q is a primary intersection point (pip). Following this definition, there are five pips in Fig. 1, namely, q_{-2}, q_{-1}, q_0, q_1 and q_2. These primary intersection points should satisfy the *Poincaré* map: $q_0=MP(q_{-2})$, $q_1=MP(q_{-1})$, $q_2=MP(q_0)$.

As shown in Fig. 1, the region on *Poincaré* section bounded by the segments of $W^u(p_1)$ and $W^s(p_2)$ connecting q_i and q_j is called a lobe if q_i and q_j are two different primary intersection points, such that there are no other primary intersection points on the segment

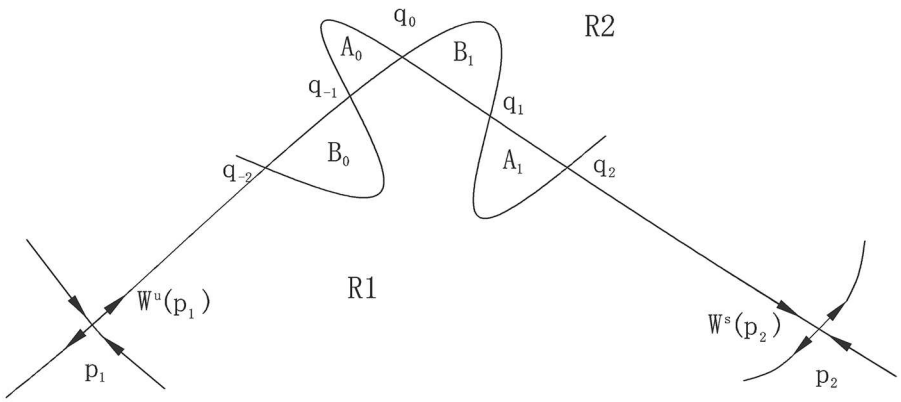

Figure 1: Lobes formed by tangling of stable manifold and unstable manifold in a periodic system.

of $W^u(p_1)$ and $W^s(p_2)$ that connect q_i and q_j. So, there are four lobes in Fig. 1, that is, A_0, B_0, A_1 and B_1. These lobes should also satisfy *Poincaré* map, $A_1=MP(A_0)$, $B_1=MP(B_0)$.

The lobes getting entrained or detrained in forward and backward time, leading to transport across these invariant manifolds, is referred to as turnstile mechanism [29]. As shown in Fig. 1, q_{-1} is the only pip between the two pips q_{-2} and q_0 in $W^s(p_1)\cap W^u(p_2)$, thus $S[q_{-2},q_0]\cup U[q_{-2},q_0]$ forms the boundary of two lobes in a precise way, one in $R1$, labeled with B_0, and the other in $R2$, labeled with A_0. Under one iteration of MP, the only points that can move from $R1$ into $R2$ by crossing the boundary B are those in B_0. Similarly, under one iteration of MP, the only points that can move from $R2$ into $R1$ by crossing B are those in A_0. After a period, lobe A_0 evolves and enters into lobe A_1, and lobe B_0 evolves and enters into lobe B_1. Therefore, transport occurs between region $R1$ and $R2$. Detailed definitions for lobe dynamics can be referred to in the literature [29].

3 Numerical method for CFD

3.1 Governing equations of unsteady flow

In this paper, the flow studied is laminar and incompressible flow because of the low *Reynolds* number. Under the condition of low *Reynolds* number, the governing equations for unsteady, incompressible, viscous flow are Navier-Stokes equations, which are given by

$$\begin{cases} \rho_f\left(\dfrac{\partial u_i}{\partial t}+u_j\dfrac{\partial u_i}{\partial x_j}\right)=-\dfrac{\partial p}{\partial x_i}+\mu\dfrac{\partial^2 u_i}{\partial x_j\partial x_j}, \\ \dfrac{\partial u_j}{\partial x_j}=0, \end{cases} \tag{3.1}$$

where ρ_f is the free stream density, μ the coefficient of dynamic viscosity, p the pressure. The Einstein summation convention is used in Eq. (3.1). The index j in Eq. (3.1) is a

dummy index which just indicates summation, and the index i is a free index. For two-dimensional flow, $i,j\in\{1,2\}$. Typically, (x_1,x_2) would be equivalent to the traditional (x,y), and u_1 and u_2 represent the velocities in the x and y direction, respectively. For the airfoil, set the chord of airfoil c be the characteristic length, free stream velocity U be the characteristic velocity. Based on the above variables, the dimensionless variables are defined as

$$x_i^*=\frac{x_i}{c},\quad t^*=\frac{Ut}{c},\quad p^*=\frac{p}{\rho_f U^2},\quad u_i^*=\frac{u_i}{U}. \tag{3.2}$$

For the sake of simplicity, the stars superscript of dimensionless variables are removed, and the standard summation conventions are used hereinafter. Then, Eq. (3.1) can be written in dimensionless form,

$$\begin{cases}\dfrac{\partial u_i}{\partial t}+u_j\dfrac{\partial u_i}{\partial x_j}=-\dfrac{\partial p}{\partial x_i}+\dfrac{1}{Re}\dfrac{\partial^2 u_i}{\partial x_j\partial x_j},\\ \dfrac{\partial u_j}{\partial x_j}=0,\end{cases} \tag{3.3}$$

where $Re=\rho_f Uc/\mu$.

3.2 Dual time stepping method and algorithm for unsteady viscous flow

In this paper, the numerical simulation of the flow around an airfoil focus on the transient process. In order to obtain more accurate results of the transient process, the dual time stepping scheme is introduced in the numerical simulation. By introducing the pseudo time, the governing equations can be written as

$$\frac{\partial u_i}{\partial\tau}+\frac{\partial u_i}{\partial t}+u_j\frac{\partial u_i}{\partial x_j}=-\frac{\partial p}{\partial x_i}+\frac{1}{Re}\frac{\partial^2 u_i}{\partial x_j\partial x_j}, \tag{3.4}$$

where τ is the pseudo time, t the real time. In each real time step, by considering the local acceleration terms as source terms, the problem becomes solving a steady solution in pseudo time tending to steady. As the solution in the pseudo time tends to be steady, namely, $\partial u_i/\partial t\to 0$, Eq. (3.4) will approach Eq. (3.3).

The characteristic based split (CBS) scheme [30] is used to solve the governing equations. By this algorithm, the first term in Eq. (3.4) is discretized along the characteristic line, which can eliminate the advection terms to avoid the numerical oscillation. The algorithm is divided into following steps,

$$\begin{cases}u_i^*-u_i^n=\Delta\tau\left[-u_j\dfrac{\partial u_i}{\partial x_j}+\dfrac{1}{Re}\dfrac{\partial^2 u_i}{\partial x_j\partial x_j}\right]^n+\dfrac{\Delta\tau^2}{2}u_k^n\dfrac{\partial}{\partial x_k}\left(\dfrac{\partial\left(u_j u_i\right)}{\partial x_j}+\dfrac{1}{Re}\dfrac{\partial^2 u_i}{\partial x_j\partial x_j}\right)^2,\\ \theta\dfrac{\partial}{\partial x_i}\left(\dfrac{\partial p^{n+1}}{\partial x_i}\right)=\dfrac{1}{\Delta\tau}\dfrac{\partial}{\partial x_i}\left(u_i^*-(1-\theta)\dfrac{\partial p^n}{\partial x_i}\right),\\ u_i^{n+1}-u_i^*=-\Delta\tau\left(\dfrac{\partial P^{n+\theta}}{\partial x_i}\right)-\Delta\tau\dfrac{3u_i^n-4u_i^N+u_i^{N-1}}{2\Delta t},\end{cases} \tag{3.5}$$

where $\Delta\tau$ is the pseudo time step, Δt the real time step, u_i^n the velocity in nth pseudo time step, u_i^N the velocity in Nth real time step, and u_i^{N-1} the velocity in real time step. Finally, the finite element method is used to solve Eq. (3.5).

3.3 Verification of numerical method

In order to verify the algorithm mentioned above for flow over the airfoil, a numerical example related to flow over NACA0012 airfoil with Re$=2000$ is simulated at different angles of attack. The numerical simulation is carried out at angles of attack $\alpha = 0^\circ - 6^\circ$, and the lift coefficients at different angles of attack are obtained. As shown in Fig. 2, it is clear that the numerical simulation results are in good agreement with the experimental results [31]. So it can be drawn that the algorithm used is available for studying the transient flow over the airfoil.

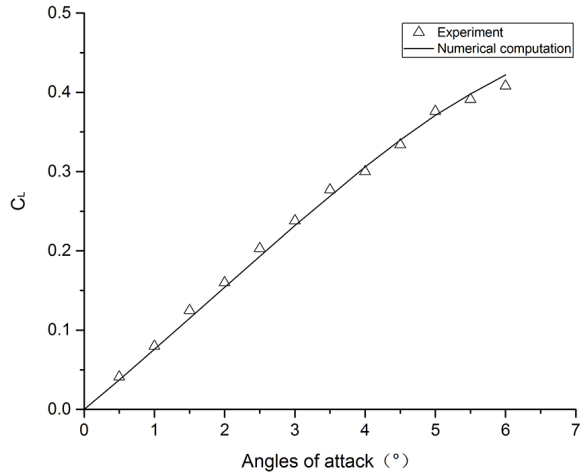

Figure 2: Comparisons between experiments and numerical results.

In order to ensure the high requirements in mesh quality, flow over the NACA0012 airfoil at Re$=5000$ and attack angle of 6 is simulated using five types of meshes, which are obtained by the Easymesh program. As shown in Table 1, it can be seen that all of the mean lift coefficients obtained from five types of meshes are close to each other. Mesh4 is chosen as the computational mesh in following studies.

4 Numerical results and discussions

The flow over NACA0012 airfoil is simulated numerically, and the Reynolds number based on the chord of airfoil is chosen as 5000. The boundary condition on the surface of

Table 1: Lift coefficients at $\alpha=6^\circ$ and Re$=5000$.

Mesh	nodes	elements	Lift coefficient
Mesh1	17026	33449	0.2774
Mesh2	21624	42685	0.2772
Mesh3	25775	50972	0.2746
Mesh4	32108	63616	0.2744
Mesh5	36235	71730	0.2741

airfoil is no-slip boundary condition, and the boundary condition on the boundary of the flow field is velocity boundary condition that is set to U.

4.1 Flow structure of separation bubble

In the case with Re$=5000$, the numerical computation is carried out at various angles of attack ($\alpha=1^\circ-8^\circ$), and Fig. 3 shows the lift coefficient versus time at each angle of attack.

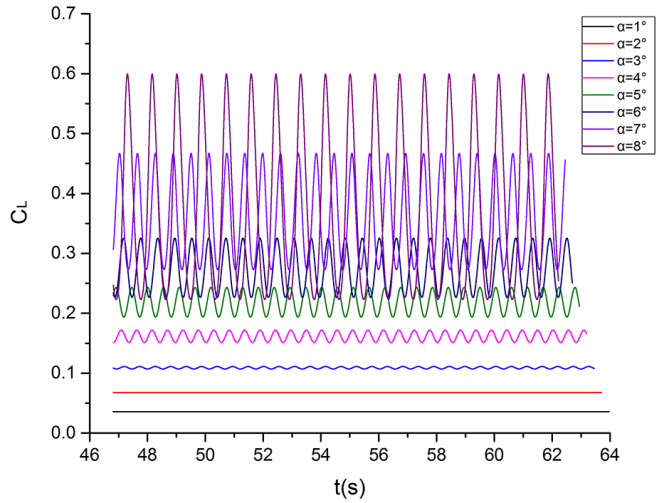

Figure 3: Lift coefficients versus time at various angles of attack.

As the angle of attack is 1° or 2°, the lift coefficient keeps constant with time, implying that the flow is steady. As the angle of attack is not less than 3°, the lift coefficient changes periodically with the time, meaning that the flow tends to be unsteady.

The velocity field information obtained from numerical simulation can be used to follow the path or trajectories of fluid particles. That is, on the basis of velocity field information, the FTLE fields in both forward and backward time can be used to capture the stable and unstable manifolds of the flow, namely, LCSs.

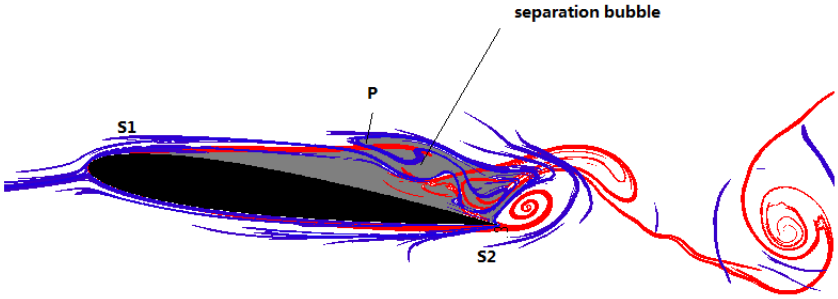

Figure 4: Separation bubble structure.

Fig. 4 shows the manifolds map of flow near NACA0012 airfoil, the red lines denote the unstable manifolds, and the blue lines the stable manifolds. The dynamic behavior of the flow can be obtained from stable manifolds near the trailing edge, and the contact point of the unstable manifold near the leading edge and the upper surface is the separation point which is denoted by $S1$. The contact point of the stable manifold near the trailing edge and the upper surface is the reattachment point which is denoted by $S2$. As shown in Fig. 4, the gray area between the separation point and reattachment point, surrounded by the stable and unstable manifolds, is a typical flow structure of separation bubble. Following lobe dynamics, P can be considered as a primary intersection point. Therefore, $\{S(P,S2)\cup U(S1,P)\}$ and the upper surface of the airfoil can be chosen as the boundary of the separation bubble from viewpoint of Lagrangian dynamics.

4.2 Mass transport in flow over airfoil

4.2.1 Lobe dynamics

Fig. 5 shows the lift coefficient of NACA0012 airfoil in a period at $\alpha=8^\circ$, T denotes the period of the lift coefficient at $\alpha=8^\circ$ ($T=0.86s$). In the following, the changes of the stable and unstable manifolds near the surface of the airfoil in a period are studied in detail, as shown in Fig. 6. And the mass transport in the process of the flow over NACA0012 airfoil is analyzed based on the lobe dynamics. In addition, the changes of position of the particles around the airfoil in a period can be used to analyze the mass transport process and verify the results obtained by lobe dynamics.

As a typical flow structure, the manifolds or lobes at moment $t=0.26T$ are chosen to analyze mass transport process. Fig. 7 shows the stable and unstable manifolds near the surface of the airfoil at $t=0.26T$. For the sake of simplicity, the schematic diagram of the manifolds near the surface of the airfoil at $t=0.26T$ is drawn in Fig. 8.

From Fig. 8, it is clear that the stable and unstable manifolds near the surface of the airfoil divides the flow into three regions, the region I, the region II and the region III.

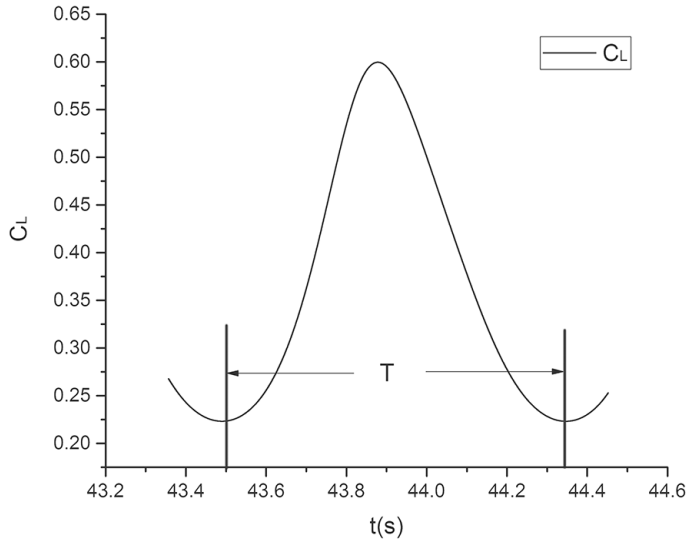

Figure 5: Lift coefficient of NACA0012 airfoil in a period at $\alpha=8^\circ$.

Among them, region I is the main flow above the airfoil and region II the main flow below the airfoil. In particular, region III, which is filled with dead-air, is the separation bubble. For the sake of clarity, separation point is denoted by $S1$ and reattachment point $S2$. Both $\{S(P,S2)\cup U(S1,P)\}$ and the upper surface of the airfoil could be chosen as the boundary of separation bubble, following the lobe dynamics. According to the lobe dynamics, it can be found there exist six primary intersection points (P_0, Q_0, P_1, Q_1, P_2 and Q_2) in the intersection points of $W^u(S1)$ and $W^s(S2)$. Further, the stable manifold and unstable manifold between two adjacent primary intersection points form the boundary of a lobe. So the tangling of $W^u(S1)$ and $W^s(S2)$ generate five lobes, namely, L_1, L_2, L_3, L_4 and L_5. As numerical computational domain is not large enough, the blue dashed line, which is a part of $W^s(S2)$ at the boundary of lobe L_1 in Fig. 8, is not shown in Fig. 7. With the evolution of time, lobe L_1 moves into the computational domain gradually, showing the whole stable manifold on the boundary of lobe L_1, such as in Fig. 6(h). Similarly, the red dotted line, which is a part of $W^u(S1)$ in Fig. 8, is not shown in the Fig. 7. From Fig. 6, it can be found that $U[A,B]$ breaks up as time goes on. In fact, if $U[A,B]$ did not break in the process of movement, then it should develop into the red dashed line. It can be seen that $U[A,B]$ has been broken in Fig. 6(f). Even if there is a fracture, the unstable manifold after breaking point B still maintains the characteristics of the unstable manifold of $S1$. On the part of the unstable manifold after the breaking point B, the lobe dynamics theory still works. Therefore, for the sake of simplicity, the red dashed line is used to replace the broken unstable manifold in Fig. 8.

In Fig. 8, mass transport between main flow and separation bubble happens, it is the result from these lobes. Obviously, the fluid elements in lobe L_1 will move to location of

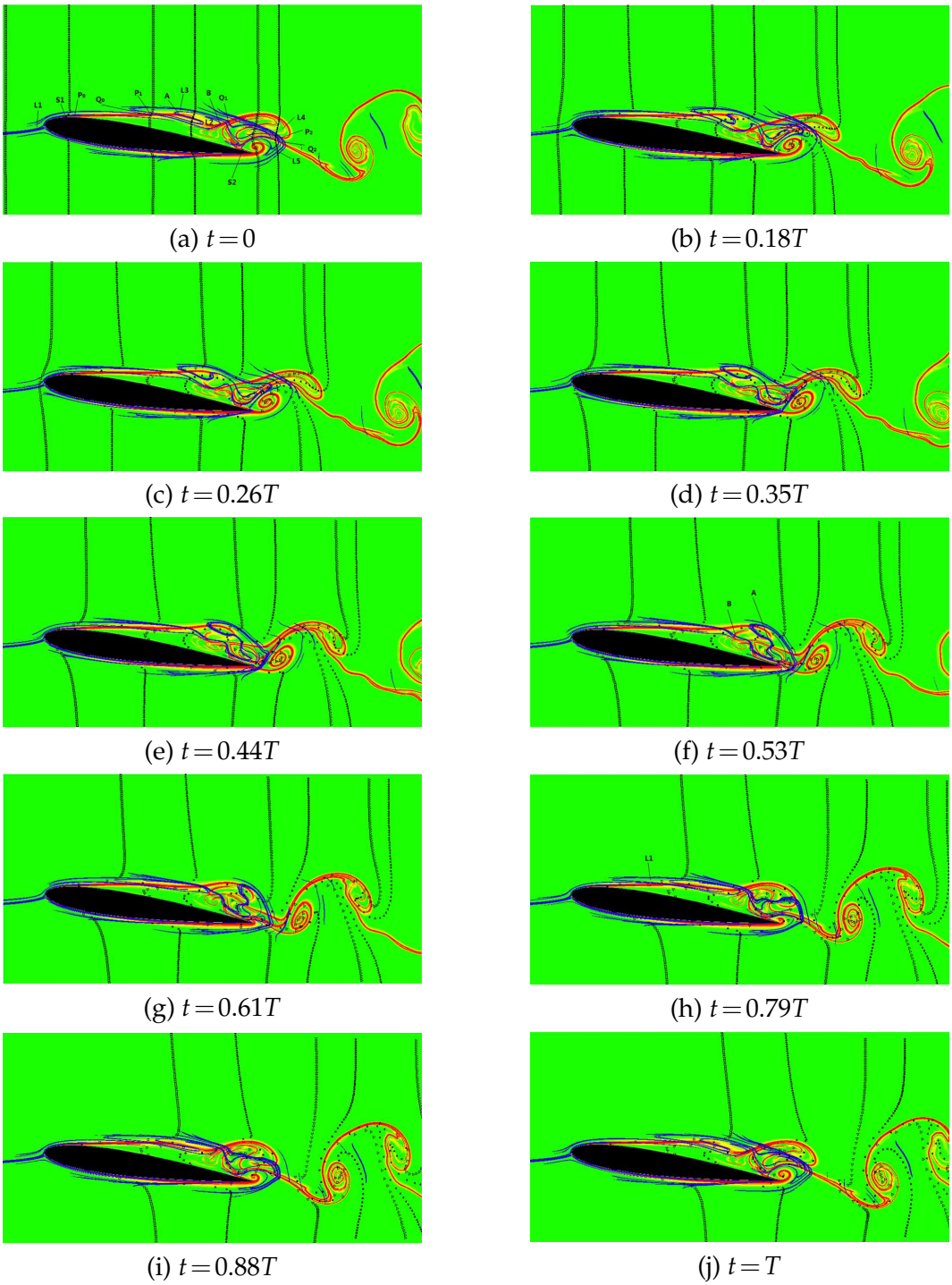

(a) $t=0$ (b) $t=0.18T$

(c) $t=0.26T$ (d) $t=0.35T$

(e) $t=0.44T$ (f) $t=0.53T$

(g) $t=0.61T$ (h) $t=0.79T$

(i) $t=0.88T$ (j) $t=T$

Figure 6: Change of stable and unstable manifolds near the surface of airfoil in a period. Six particle groups are taken in the vicinity of the airfoil, □ (the first group), ▲ (the second group), ▽ (the third group), ■ (the fourth group), ▷ (the fifth group) and ◀ (the sixth group).

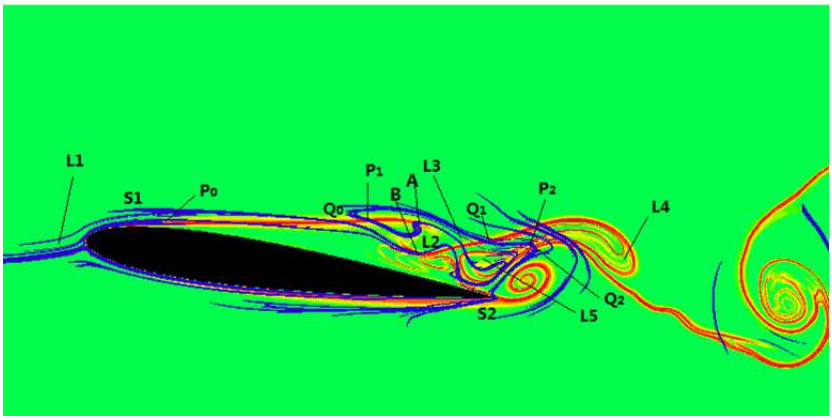

Figure 7: Stable and unstable manifolds near the surface of airfoil at $t=0.26T$.

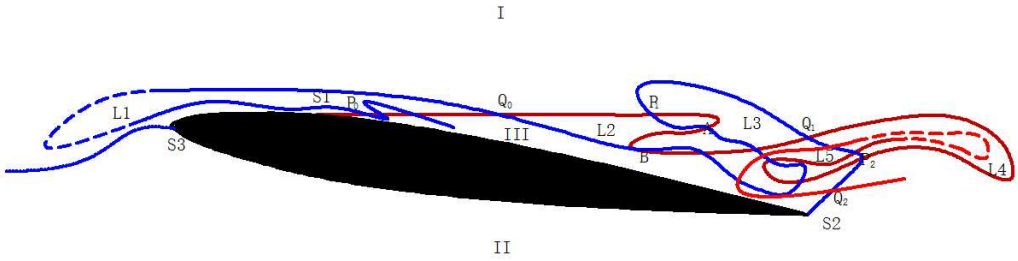

Figure 8: Schematic diagram of stable and unstable manifolds near the surface of airfoil at $t=0.26T$ (the red lines denote the unstable manifolds, and the blue lines the stable manifolds).

lobe L_3 after a period. With the evolution of time, lobe L_1, located in the main flow region I, enters the separation bubble. Similarly, the fluid in lobe L_2 will move to the location of lobe L_4 after a period, and then lobe L_2, located in the separation bubble, enters the main flow region I. Clearly, the fluid entering the separation bubble is mainly derived from the boundary layer in upstream. That is the mass transport which could not be described by Eulerian description.

4.2.2 Verification by motions of particle groups

In order to verify the results of lobe dynamics, we are now refer to Fig. 6 which shows the changes of stable and unstable manifolds and the position of the particles around the surface of the airfoil in a period. As shown in the Fig. 6, six particle groups are taken in the vicinity of the airfoil at $t=0$.

It is clear that the particles far away from the airfoil are moving horizontally along the direction of the main flow. In the whole period, there is a singular point $S3$ in front of airfoil. Following the physical meaning, LCSs can be considered as the boundary or barriers of the flow area, the stable manifold of $S3$ divides the fluid near the leading edge

of the airfoil into two regions: region I and region II, as mentioned above. The fluid in region I flows over the airfoil to the downstream, and the fluid in region II flows beneath the airfoil. As a conclusion, it can be drawn that the stable manifold of $S3$ divides the fluid near the leading edge of the airfoil into two regions by the motion of the first particle group. Fluid particles near separation point $S1$ at $t=0$ flow along unstable manifold near $S1$ and do not pass through the unstable manifold near $S1$ in the whole period. So, $S1$ can be used as the separation point of airfoil surface. There is a dead-air zone below the unstable manifold near to $S1$, so that the fluid particles in this zone move slowly.

Fig. 6 shows that the first particle group in lobe L_1 at $t=0$ moves to area above the airfoil at $t=0.26T$, and eventually the fluid in the lobe L_1 moves to the position of lobe L_3.

By observing the boundary of lobe L_2 and the third particle group located in lobe L_2, it can be seen that the fluid in lobe L_2 rotates counterclockwise near the trailing edge, and the fluid moves upstream then moves downstream reaching lobe L_4 at the end of the period. As a result, lobe L_2 carries the fluid from separation bubble to the main flow. In the same way, it can be seen that the fluid in lobe L_4 falls off and becomes a clockwise vortex which will shed in the wake. Therefore, the fluid in lobe L_2 will arrive in lobe L_4 and then will shed in the wake.

However, there is a special zone in both lobe L_2 and lobe L_3. That is, the boundary of this zone breaks in the process of lobe L_2 reaching to lobe L_4, leading to a mixture of the fluid in this zone and the fluid remained in lobe L_2. On the other hand, the remaining fluid in lobe L_3 is gradually close to the trailing edge of the airfoil and moves clockwise to the inner of the separation bubble.

There is an interesting phenomenon, that is, the position of the separation point does not change in the whole period, while the position of the reattachment changes over time. There are a short distance and a counter clockwise vortex between the reattachment point and tip point of the airfoil at $t=0$. Over the period, the vortex moves backwards, and the reattachment point moves to the tip of the airfoil as the vortex moves backwards.

When $t=0.35T$, the vortex completely leaves the upper surface of the airfoil and moves to downstream, and the separation point also moves to the trailing edge of the airfoil.

Then, when $t=0.53T$, the fluid from the lower surface of the airfoil moves over the trailing edge of the airfoil and moves to the upper surface of airfoil. A new counter clockwise vortex is generated, and the volume of the new vortex begins to increase with time. That is the reason that the reattachment point moves forward.

When $t=T$, the position of reattachment point is same as the position of reattachment point at $t=0$, and the distribution of manifolds is exactly the same as that at $t=0$. In this process, the reattachment point position on the upper surface of the airfoil changes periodically, and the period is also equals T.

Through the analyses above, it can be found that the results obtained by lobe dynamics are much more intuitive than the kinetic description, such as streamline etc.

4.3 Relationship between mass transport and lift

4.3.1 Distributions of pressure coefficient of NACA0012 airfoil

Fig. 9 shows the distributions of pressure coefficient of NACA0012 airfoil in a period at $\alpha = 8^\circ$. The flow is divided into 3 parts with the airfoil chord length. The part that chord length range from 0 to 0.2c is the front of the airfoil; The part that chord length range from 0.2c to 0.7c is the central section of the airfoil; The part that chord length range from 0.7c to c is the rear of the airfoil. It can be obtained from Fig. 10 that the distribution of the pressure coefficient in the front of airfoil in the whole period remains unchanged. However, the distributions of the pressure coefficient in the central section and rear of airfoil change with time. Especially, the pressure coefficient in the rear of the airfoil changes intensely. In addition, the distribution curve of the pressure coefficient at $t = 0$ is completely coincident with that at $t = T$.

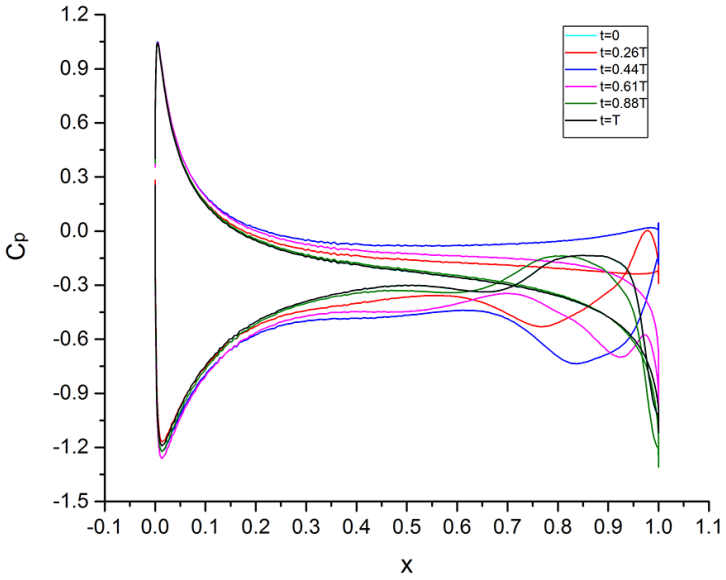

Figure 9: Distributions of pressure coefficient at various time in a period (Re$=5000$, $\alpha = 8^\circ$).

When $t = 0$, the pressure is higher on the upper surface at rear of the airfoil than that on the lower surface at the rear of the airfoil. On the trailing edge, the pressure of upper and lower surface is very low.

When $t = 0.26T$, the pressure on the lower surface of the central section is risen, and the pressure on the upper surface of the central section is decreased. The length of the area where the pressure on the upper surface is higher than that on the lower surface is reduced greatly, and this area is getting close to the trailing edge. And the pressure on the airfoil is raised near the trailing edge.

When $t=0.44T$, the area where the pressure on the upper surface is higher than that on the lower surface is completely disappeared. The pressure on the lower surface of the central section and rear is obviously increased. Therefore, in the first half of the period, the lift coefficient of the airfoil is enhanced. When $t=0.61T$, the pressure on the upper surface of the central section is risen, and the pressure on the lower surface of the central section begins to drop. The pressure on the upper and lower surface near the trailing edge of the airfoil is also reduced greatly.

When $t=0.88T$, the pressure on the upper surface of the central section is still rising, and the pressure on the upper surface of the central section remains dropping. Also, the pressure on the upper surface of the rear is rising, and the pressure on the upper surface of the rear remains dropping. The area where the pressure on the upper surface is higher than that on the lower surface appears again. Consequently, the volume of this area is increasing. When $t=T$, the pressure distribution on the airfoil surface is exactly the same as that at $t=0$. Accordingly, the lift coefficient of the airfoil is decreased in the second half of the period. In each of the following periods, the variation of the pressure coefficient and the lift coefficient of the airfoil surface is exactly the same as that described above.

4.3.2 Relationship between mass transport and lift

In a period, the unstable manifold near the leading edge keeps constant mostly, indicating that there is no mass transport between the front region of the separation bubble III and the main flow region I. So the energy exchange between the front region of the separation bubble III and the main flow I mainly depends on the molecular diffusion. The fluid in this region is greatly influenced by viscosity, meaning there exists a large area of dead air near airfoil surface.

In Fig. 8, when $t=0$, the fluid in the lobe L_3, which is in the separation bubble (region III), is derived from the main flow (region I). The fluid in the lobe L_3 is near to the central section of the airfoil at $t=0$, then the fluid moves to the rear of the airfoil and mixes with the fluid in the separation bubble as the time evolution. The mean velocity of the fluid in the main flow is higher than that in the separation bubble. Through the mass transport between main flow and separation bubble, the kinetic energy and the momentum of the fluid in the separation bubble are enhanced, and the pressure is dropped. The fluid in both lobes L_2 and L_3 moves to lobe L_4 and leaves the separation bubble, and eventually the fluid sheds to the wake and falls off as a clockwise vortex. As the results, pressure in separation bubble is raised, and the lift coefficient is increased in the first half period and decreased in the second half period.

The pressure of the upper surface near the trailing edge is increased in the first half period and decreased in the second half period, which is mainly influenced by the counter clockwise vortex near the trailing edge. The fluid in this vortex is composed of fluid from the main flow (region II). In the process of the vortex formation, the mean velocity of the surrounding fluid is increased, and the pressure on the upper surface of the airfoil near the vortex can be reduced. On the contrary, in the process of vortex shedding, the pressure on the upper surface of the airfoil near the vortex can be increased. However,

the effect from the mass transport on the lift coefficient is more powerful than the effect of the vortex on the lift coefficient. Therefore, the lift coefficient of the airfoil is mainly controlled by the mass transport process in the main flow and the separation bubble.

5 Conclusion

LCSs and lobe dynamics are introduced to investigate the mass transport between separation bubble and main flow, from viewpoint of nonlinear dynamics. The structures of the separation bubble from viewpoint of Lagrangian dynamics are shown by LCSs, and the position of the reattachment point on the upper surface of the airfoil changes periodically, as well the lift coefficient. The results show that stable manifolds and unstable manifolds could be tangled with each other as time evolution, and the lobes are formed periodically to induce mass transport between main flow and separation bubble. Moreover, the evolution of the separation bubble depends essentially on the mass transport which is induced by lobes. Also, the lift coefficient of the airfoil is mainly controlled by the mass transport process in the main flow and the separation bubble. As a conclusion, it can be drawn that the flow separation could be studied by LCSs and lobe dynamics, and the flow separation could be controlled feasibly if an appropriate control is applied to the upstream boundary layer with high momentum from the main flow.

Besides, mass transport and energy exchange exists widely in oceanic flow, atmospheric flow and heat transport process. It is valuable to study these problems. Looking to the future,the LCS and lobe dynamics can be used to study the problem of air pollutants and the ocean flow, and maybe it is likely to be used to study the heat transfer problem.

Acknowledgments

This work is supported by National Key fundamental Research Program of China (973 Program, No. 2012CB026002), and the National Natural Science Foundation of China (No. 51305355).

References

[1] H. P. Horton. *Laminar separation bubbles in two and three dimensional incompressible flow.* PhD thesis, 1968.
[2] T. J. Mueller and S. M. Batil. Experimental studies of separation on a two-dimensional airfoil at low Reynolds numbers. *AIAA journal*, 20(4):457–463, 1982.
[3] M. O'meara and T. J. Mueller. Laminar separation bubble characteristics on an airfoil at low Reynolds numbers. *AIAA journal*, 25(8):1033–1041, 1987.
[4] M. Gaster. *The structure and behaviour of laminar separation bubbles*. Citeseer, 1969.
[5] J. C. M. Lin and L. L. Pauley. Low-Reynolds-number separation on an airfoil. *AIAA journal*, 34(8):1570–1577, 1996.

[6] S. Yarusevych, P. E. Sullivan, and J. G. Kawall. On vortex shedding from an airfoil in low-Reynolds-number flows. *Journal of Fluid Mechanics*, 632:245–271, 2009.
[7] J. Egambaravel and R. Mukherjee. Linear stability analysis of laminar separation bubble over NACA0012 airfoil at low Reynolds numbers.
[8] D. A. Hammond and L. G. Redekopp. Local and global instability properties of separation bubbles. *European Journal of Mechanics-B/Fluids*, 17(2):145–164, 1998.
[9] U. Rist and U. Maucher. Investigations of time-growing instabilities in laminar separation bubbles. *European Journal of Mechanics-B/Fluids*, 21(5):495–509, 2002.
[10] G. S. Schmidt and T. J. Mueller. Analysis of low Reynolds number separation bubbles using semiempirical methods. *AIAA journal*, 27(8):993–1001, 1989.
[11] J. H. Almutairi, L. E. Jones, and N. D. Sandham. Intermittent bursting of a laminar separation bubble on an airfoil. *AIAA journal*, 48(2):414–426, 2010.
[12] Y.K. Shum and D.J. Marsden. Separation bubble model for low Reynolds number airfoil applications. *Journal of aircraft*, 31(4):761–766, 1994.
[13] L. L. Van Dommelen and S. J. Cowley. On the Lagrangian description of unsteady boundary-layer separation. Part 1. General theory. *Journal of Fluid Mechanics*, 210:593–626, 1990.
[14] K. Shariff, T. H. Pulliam, and J.M. Ottino. A dynamical systems analysis of kinematics in the time-periodic wake of a circular cylinder. *Lect. Appl. Math*, 28:613–646, 1991.
[15] J. Duan and S. Wiggins. Lagrangian transport and chaos in the near wake of the flow around an obstacle: a numerical implementation of lobe dynamics. *Nonlinear Processes in Geophysics*, 4(3):125–136, 1997.
[16] G. Haller. Finding finite-time invariant manifolds in two-dimensional velocity fields. *Chaos: An Interdisciplinary Journal of Nonlinear Science*, 10(1):99–108, 2000.
[17] G. Haller. Lagrangian coherent structures from approximate velocity data. *Physics of Fluids (1994-present)*, 14(6):1851–1861, 2002.
[18] S. C. Shadden, F. Lekien, and J. E. Marsden. Definition and properties of Lagrangian coherent structures from finite-time Lyapunov exponents in two-dimensional aperiodic flows. *Physica D: Nonlinear Phenomena*, 212(3):271–304, 2005.
[19] P. Lei, J. Zhang, K. Li, and D. Wei. Study on the transports in transient flow over impulsively started circular cylinder using Lagrangian coherent structures. *Communications in Nonlinear Science and Numerical Simulation*, 22(1):953–963, 2015.
[20] G. Haller. Exact theory of unsteady separation for two-dimensional flows. *Journal of Fluid Mechanics*, 512:257–311, 2004.
[21] A. Surana and G. Haller. Ghost manifolds in slow-fast systems, with applications to unsteady fluid flow separation. *Physica D: Nonlinear Phenomena*, 237(10):1507–1529, 2008.
[22] F. J. Beron-Vera, M. J. Olascoaga, and G. J. Goni. Oceanic mesoscale eddies as revealed by Lagrangian coherent structures. *Geophysical Research Letters*, 35(12), 2008.
[23] M. Mathur, G. Haller, T. Peacock, J. E. Ruppert-Felsot, and H. L. Swinney. Uncovering the Lagrangian skeleton of turbulence. *Physical Review Letters*, 98(14):144502, 2007.
[24] A. E. BozorgMagham, S. D. Ross, and D. G. Schmale. Real-time prediction of atmospheric Lagrangian coherent structures based on forecast data: an application and error analysis. *Physica D: Nonlinear Phenomena*, 258:47–60, 2013.
[25] G. Haller and G. Yuan. Lagrangian coherent structures and mixing in two-dimensional turbulence. *Physica D: Nonlinear Phenomena*, 147(3):352–370, 2000.
[26] G. Haller. A variational theory of hyperbolic Lagrangian coherent structures. *Physica D: Nonlinear Phenomena*, 240(7):574–598, 2011.
[27] D. Lipinski and K. Mohseni. A ridge tracking algorithm and error estimate for efficient com-

putation of Lagrangian coherent structures. *Chaos: An Interdisciplinary Journal of Nonlinear Science*, 20(1):017504, 2010.

[28] A. M. Mancho, D. Small, S. Wiggins, and K. Ide. Computation of stable and unstable manifolds of hyperbolic trajectories in two-dimensional, aperiodically time-dependent vector fields. *Physica D: Nonlinear Phenomena*, 182(3):188–222, 2003.

[29] N. Malhotra and S. Wiggins. Geometric structures, lobe dynamics, and Lagrangian transport in flows with aperiodic time-dependence, with applications to rossby wave flow. *Journal of nonlinear science*, 8(4):401–456, 1998.

[30] P. Nithiarasu. An efficient artificial compressibility (AC) scheme based on the characteristic based split (CBS) method for incompressible flows. *International Journal for Numerical Methods in Engineering*, 56(13):1815–1845, 2003.

[31] P. J. Kunz. *Aerodynamics and design for ultra-low Reynolds number flight*. PhD thesis, Stanford University, 2003.

[32] D. Lipinski, B. Cardwell, and K. Mohseni. A Lagrangian analysis of a two-dimensional airfoil with vortex shedding. *Journal of Physics A: Mathematical and Theoretical*, 41(34):344011, 2008.

[33] S. Yarusevych, P. E. Sullivan, and J. G. Kawall. Coherent structures in an airfoil boundary layer and wake at low Reynolds numbers. *Physics of Fluids (1994-present)*, 18(4):044101, 2006.